EFFECT OF THE DIRECTION OF AN EXTERNAL APPLIED MAGNETIC FIELD ON THE MICROMAGNETIC PROPERTIES OF Fe CUBOIDS

EFECTO DE LA DIRECCIÓN DE UN CAMPO MAGNÉTICO EXTERNO APLICADO SOBRE LAS PROPIEDADES MICROMAGNÉTICAS DE CUBOIDES DE Fe

Mauricio Galvis-Patiño, Johans Restrepo-Cárdenas

Grupo de Magnetismo y Simulación G+, Instituto de Física, Universidad de Antioquia, A.A. 1226, Medellín, Colombia.

(Recibido: 12/2021. Aceptado: 06/2022)

Abstract

We present the results of the study of the micromagnetic properties and the magnetization dynamics of a system of Fe cuboids with a square base of length, $L = 120$ nm and thickness, $t = 9$ nm, under free boundary conditions as a function of the angle of an in-plane applied external magnetic field, for which we have used the Ubermag micromagnetic program that uses the OOMMF package and the finite difference method with a cell size, $c = 3$ nm. Hysteresis loops show that the coercive field (H_c) decreases with increasing azimuthal angle, from one easy-magnetizing axis to the other; in turn, the remanent magnetization (M_r) remains constant and magnetization diagrams indicate the presence of magnetic domains and walls in the (x, y) plane, accompanied by a magnetization component that points, both, outward and inward of the plane. This behavior is associated with the type of anisotropy and the aspect ratio of the cuboid. Finally, energy graphs show how the competition between the dipole (E_d), the exchange (E_{ex}), anisotropy (E_K), and Zeeman (E_Z) energies occurs along the hysteresis loops.

Mauricio Galvis: mauricio.galvisp@udea.edu.co https://doi.org/10.15446/mo.n65.100454

Keywords: cuboid, micromagnetic program, finite differences, hysteresis loops.

Resumen

Presentamos los resultados del estudio de las propiedades micromagnéticas y la dinámica de la magnetización de un sistema de cuboides de Fe de base cuadrada de longitud $L = 120$ nm y espesor $t = 9$ nm, bajo condiciones de frontera libre en función del ángulo de un campo magnético externo aplicado en el plano, para lo cual hemos utilizado el programa micromagnético Ubermag, que utiliza el paquete OOMMF y el método de diferencias finitas con un tamaño de celda $c = 3$ nm. Los ciclos de histéresis muestran que el campo coercitivo (H_c) disminuye con el aumento del ángulo azimutal, desde un eje de fácil magnetización hasta el otro; a su vez, la magnetización remanente (M_r) permanece constante y los diagramas de magnetización indican la presencia de dominios y paredes de dominio magnético en el plano (x, y), acompañados de una componente de magnetización que apunta tanto hacia fuera como hacia dentro del plano. Este comportamiento está asociado al tipo de anisotropía y a la relación de aspecto del cuboide. Por último, los gráficos de energía muestran cómo se produce la competencia entre las energías dipolar (E_d), intercambio (E_{ex}), anisotropía (E_K) y Zeeman (E_Z) a lo largo de los ciclos de histéresis.

Palabras clave: cuboide, programa micromagnético, diferencias finitas, ciclos de histéresis.

Introduction

Currently, the study of the magnetic properties of Fe systems presents a great interest by research groups due to its applications in medicine, technology and chemical sensors [1] - [2]. The study of this kind of structures at a microscopic level seeks to understand the different mechanisms of magnetization inversion and the relationship between size, shape, physical parameters and material properties that largely determine their uses [3] - [4].

Moreover, the magnetization processes of nanoscale Fe systems under the action of a static external magnetic field are determined by the competition between exchange, dipole, anisotropy and Zeeman energies [5], which try to reach their equilibrium state, giving rise to various mechanisms involved in the magnetization and demagnetization processes of the system, together with the movement of the domain walls, as the vortex-type state (V). This is characterized by a core morphology of the magnetic domain walls, which allows identifying the presence of vortex-type states (V) with motion capability with magnetic moments around them, and single-domain (SD) states governed by a coherent magnetization rotation [6].

Previous studies of nanostructures with various geometries and sizes have shown that there is a direct relationship between the angle at which the external magnetic eld is applied and the coercive force [7].

Model and methodological aspects

A square base cuboid Fe system with free boundary conditions, with an edge of 120 nm and a thickness of 9 nm was considered. The physical input parameters of Fe are presented in Table 1.

Property	**Value**
Anisotropy Constant (K_1)	48 kJ/m^3
Anisotropy Type	Cubic
Crystalline Planes	[100]/[010]
Exchange Stifness (A_x)	21 pJ/m
Damping Constant (α)	1.0
Saturation Magnetization (M_s)	1.7 MA/m
Discretization Cell	3 nm

TABLE 1. Physical input parameters for Fe [8].

Initially a $\pm$160 mT (step of 5 mT) field was applied in the x direction, which corresponds to one of the easy magnetization axis, then the field was applied in a coplanar way to the (x, y) plane under angles from 0° to 180° with steps of 15° in regard to the x axis (Fig. 1).

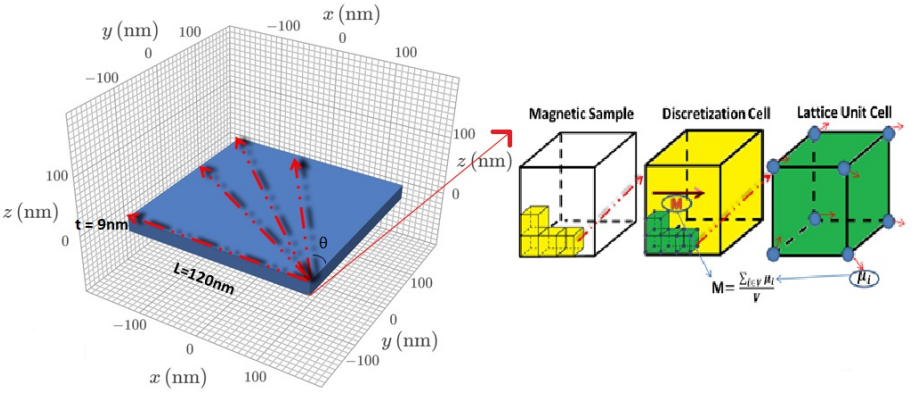

FIGURE 1. *Graphical representation of the sample and the finite differences method for a Fe cuboid of* 120 *nm of edge and thickness of* 9 *nm.*

The micromagetic simulations were carried out through the Ubermag program, which is a backend to drive existing micromagnetic simulators in a Python environment and within the Jupyter Notebook. Likewise, we use the method of finite differences with which we have discretized all the sample volume in small cuboids of edge of 3 nm (Fig. 1). In order to obtain reliable results, such a discretization cell must be smaller than the exchange length [9], given by:

$$l_{ex} = \sqrt{2A/(\mu_0 M_s^2)} = 3.4nm \tag{1}$$

where $A = 2.1 \times 10^{-11}$ J/m is the constant exchange stifness, $M_s = 1.7 \times 10^6$ A/m represents the saturation magnetization and μ_0 the permeability of free space.

As for the dynamics of time-dependent magnetization, this was solved with the open source OOMMF (Object Oriented MicroMagnetic Framework), *software* developed by the National Institute of Standards and Technology (NIST) Donahue and Porter [10]; program that solves the differential equation of Landau-Lifshitz-Gilbert (LLG) [11], given by:

$$\frac{d\mathbf{m}}{dt} = \underbrace{-\gamma_0(\mathbf{m} \times \mathbf{H}_{eff})}_{precession} + \underbrace{\alpha\left(\mathbf{m} \times \frac{d\mathbf{m}}{dt}\right)}_{damping}. \tag{2}$$

The first and second terms of this equation represent respectively the precession of the magnetization vector M around the effective field (H_{eff}) and the dissipation of this one, where $\gamma_0 = \mu_0\gamma = 2.211\times10^5$ mA$^{-1}s^{-1}$, γ is known as the gyromagnetic ratio, $\alpha = 1$ is Gilbert's damping constant, [12] and $\mathbf{m} = \mathbf{M}/\mathbf{M_s}$ is the normalized magnetization. On the other hand, the effective field is:

$$\mathbf{H}_{eff} = -\frac{1}{\mu_0 M_s}\frac{\delta w(\mathbf{m})}{\delta \mathbf{m}} \tag{3}$$

Being $w(\mathbf{m})$ the energy density functional of the system:

$$w(\mathbf{m}) = w_1 + w_2 + w_3 + ... = \sum_{i=1} w_i(\mathbf{m}) \tag{4}$$

By integrating over the volume of the sample, the total energy is obtained:

$$E[\mathbf{m}] = \int_v w(\mathbf{m})dV \tag{5}$$

Therefore, the Hamiltonian of the system is:

$$\mathcal{H} = -A\mathbf{m}\cdot\nabla^2\mathbf{m} - K[(\mathbf{m}\cdot\mathbf{u}_1)^2(\mathbf{m}\cdot\mathbf{u}_2)^2 + (\mathbf{m}\cdot\mathbf{u}_2)^2(\mathbf{m}\cdot\mathbf{u}_3)^2 + (\mathbf{m}\cdot\mathbf{u}_3)^2(\mathbf{m}\cdot\mathbf{u}_1)^2] - \frac{1}{2}\mu_0 M_\mathrm{s}\mathbf{m}\cdot\mathbf{H}_\mathrm{d} - \mu_0 M_\mathrm{s}\mathbf{m}\cdot\mathbf{H} \tag{6}$$

where A is the exchange constant; $\mathbf{u_1}$, $\mathbf{u_2}$, and $\mathbf{u_3}$ are unit vectors and represent the three axes of easy magnetization associated with the cubic anisotropy of iron; $\mathbf{H_d}$ is the demagnetizing field due to the magnetostatic interaction, and $\mathbf{H}$ is the external applied magnetic field.

Results and Discussion

Figure 2 shows square hysteresis loops that are typical of a ferromagnetic material as expected for iron. The most relevant feature is the fact that, despite of having well-defined easy axes, namely the [1 0 0] and [0 1 0], the system becomes even magnetically softer as the external field is applied along a direction resulting from a linear combination of these two directions. For $\theta = 0°$

and 90°, for which the hysteresis loops are the same and the field direction coincides to those ones of the easy axes, coercive forces, even though small, are greater than those obtained for intermediate angles. A reasonable explanation can be given in terms of the possible paths that the system can follow along the phase space in order to minimize its energy, which we analyze below. When the field points out along an easy axis ($\theta = 0°$ and 90°), magnetization reversal tends to occur by the nucleation and propagation of a Néel wall. In contrast, in the case of the field applied along intermediate angles, different paths of microstates can be followed, facilitating the mechanism of magnetization, switching and decreasing the coercive force. These features are in turn enhanced by the 3D character of the sample, where the accessibility to more microstates, compatible with the macrosted (H, M) of the system, is more limited.

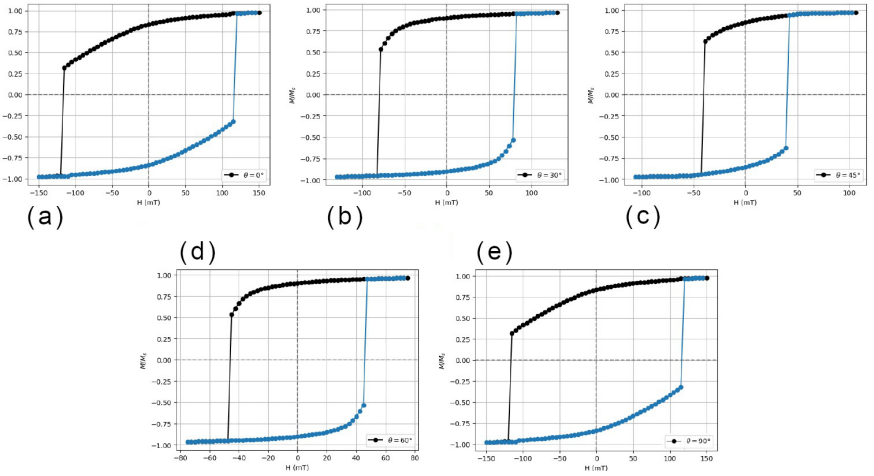

FIGURE 2. *Hysteresis loops obtained for Fe cuboids with $t = 9$ nm and angles of: a) 0°, b) 30°, c) 45°, d) 60° and e) 90°. The branch of the decreasing field is represented by the black circles, whereas the branch of the increasing field by blue circles.*

Summarizing, a reduction of the coercive field is observed with the increase of the angle of the field. However for an angle of 90 $\mathring{A}$ a maximum value is again achieved, because the magnetic moments are oriented with the external field applied along one of the easy magnetization axes (Fig. 3), and the process is then repeated.

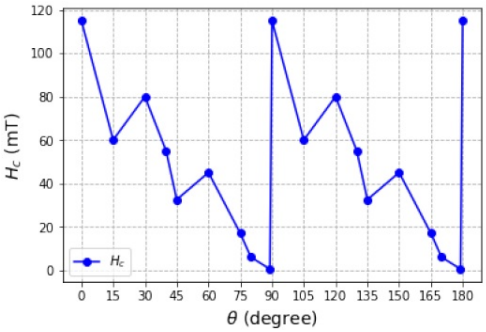

FIGURE 3. *Coercive field as a function of the applied external magnetic field angle of Fe cuboids with* $L = 120\ nm$, $t = 9\ nm$ *for angles between* 0° *and* 180°.

Angle	**Maximum Value (J)**				**Minimum Value (J)**			
	Ed	**Eex**	**Ek**	**Ez**	**Ed**	**Eex**	**Ek**	**Ez**
	(10^{-17})	(10^{-18})	(10^{-18})	(10^{-17})	(10^{-17})	(10^{-18})	(10^{-18})	(10^{-17})
0	1.58	6.01	4.47	0.98	1.05	0.84	0.26	-3.32
30°	1.36	6.25	- 0.62	1.15	1.16	0.98	- 0.94	- 3.30
45°	1.36	3.41	- 0.59	0.75	1.18	0.88	- 1.23	- 3.25
60°	1.37	6.25	- 0.68	1.23	1.16	0.98	- 0.96	- 3.25
90°	1.58	6.01	4.47	0.98	1.05	0.84	0.26	- 3.32

TABLE 2. *Energy values for diferent angles.*

To contextualize all the above aspects, an analysis of the different energy contributions is summarized in Table 2, where the minimum and maximum values have been recorded. Starting at H = 150 mT, a well-defined saturation state (M_s) is observed with the moments oriented parallel along the same direction. This configuration causes a minimum in the anisotropy, exchange, and Zeeman energies due to the almost parallel orientations of the magnetic moments and concomitantly a maximum in the demagnetizing energy due to the absence of domains and walls as can be observed in Figure 4. Nevertheless, the scale and magnitude of such values depends on the angle and they are listed in Table 2. As we move along the upper branch (black dots) of the hysteresis loops towards negative values of the field, the anisotropy, exchange, and Zeeman energies increase as the magnetic moments begin to rotate in

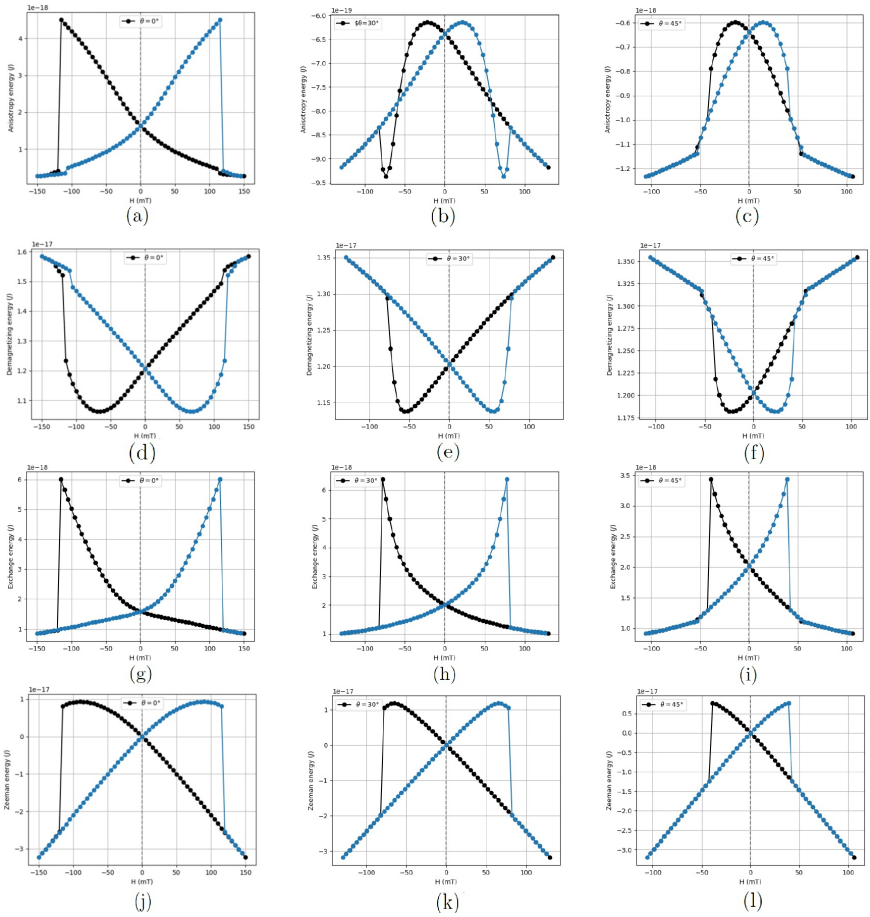

FIGURE 4. *Energy diagrams obtained with $L = 120$ nm, $t = 9$ nm for angles of $0°$: a) E_k, d) E_d, g) E_{ex} and j) E_Z. $30°$: b) E_k, e) E_d, h) E_{ex} and k) E_Z and $45°$: c) E_k, f) E_d, i) E_{ex} and l) E_Z. The decreasing field branch is represented by the black circles, while the increasing field branch is represented by the blue circles.*

different directions in an attempt of minimizing the magnetostatic energy by forming domains. This diminishes the demagnetizing energy in a closely linear fashion. Before reaching the coercive force, the demagnetizing energy reaches a minimum due to a damping in the movement of the domain walls to then continue moving in opposite directions causing an increase in E_d. Once the coercive force is achieved, the magnetization reversal takes place and the energies undergo a sharp change. In this last stage, before

reaching negative saturation $(-M_s)$, the domain walls are widely displaced to allow those domains, with the principal component of magnetization parallel to the field direction, to acquire a larger size, resulting in coalescence of the domains to reach the saturation state.

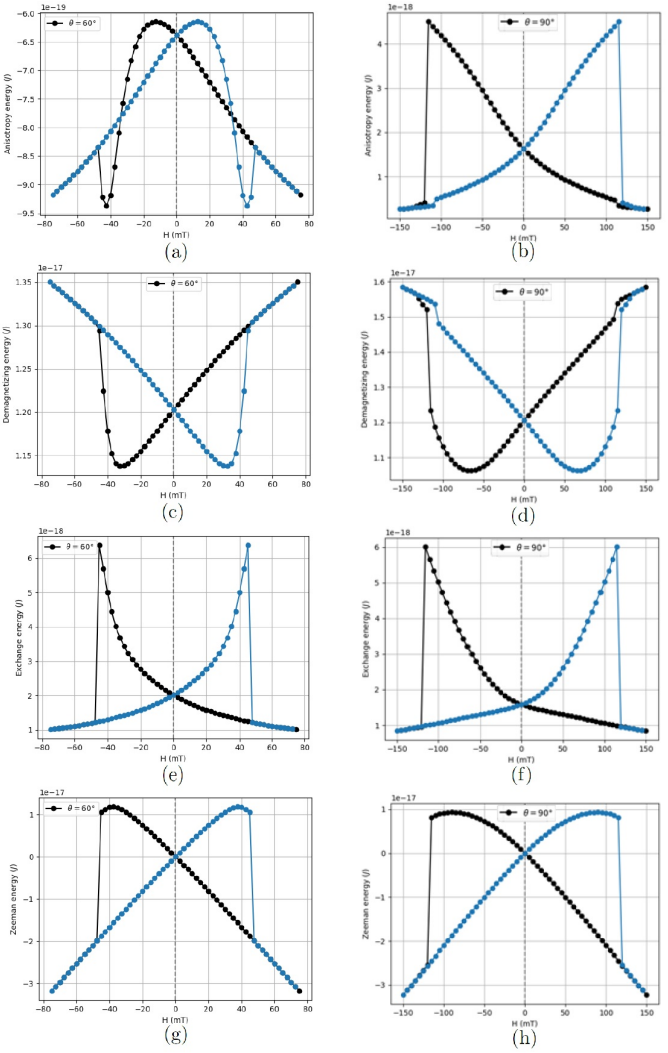

FIGURE 5. *Energy diagrams for $L = 120$ nm, $t = 9$ nm for angles of 60°: a) E_k, c) E_d, e) E_{ex} and g) E_Z and 90°: b) E_k, d) E_d, f) E_{ex} and h) E_Z. The decreasing field branch is represented by the black circles, while the increasing field branch is represented by the blue circles.*

All the above observations are qualitatively common for all the angles. Such a minimum is even smaller than the corresponding one to the saturation state and it is related with the hump observed in the coercive force for this angle (see Fig. 3). This indicates that the reversal mechanisms of magnetization are sensitive to the field orientation. The corresponding results for another aspect ratio, namely the one with $L = 120$ nm and $t = 9$ nm, are shown in Figure 5, where the same general behavior is observed. We want to emphasize the orders of magnitude of the energies. As observed, the anisotropy and exchange energies are one order of magnitude smaller than the magnetostatic and Zeeman energies away from the zero field. This means that most of the observed phenomenology is ruled mainly by the latter two energy terms.

An interesting feature occurs for $\theta = 30°$ and $\theta = 60°$, where a small increase of the coercive field is observed. This behavior can be associated to the magnetization process marked by magnetic moments pointing perpendicularly both in the center of the cuboid and at its edges, in addition to coplanar magnetic moments between these two orientations, which generates a greater amount of magnetic domain walls.

Finally, a set of snapshots corresponding to the magnetic configurations at some selected field values, along the loop, are shown in Figure 6. For an angle of 0° and a field of H $\sim \pm 145$ mT most of the magnetic moments lie on the (x, y) plane, oriented in the same sense and direction as the applied field, close to an equilibrium saturation state (M_s). At the edges of the cuboid, some small regions with z-magnetization component pointing out-of-plane (positive and negative) are observed. This is a free boundary effect due to finite size of the system, which favors the formation of domains [13]. At $H \sim 0mT$, the magnetic domains grow in such a way that three large regions of magnetization are evident: the first one in the (x, y) plane in the same direction and sense as the applied field, which is associated with the remanence of the material; the second one on the left side of the cuboid, pointing out of the plane, and the third one on the right side of the cuboid,

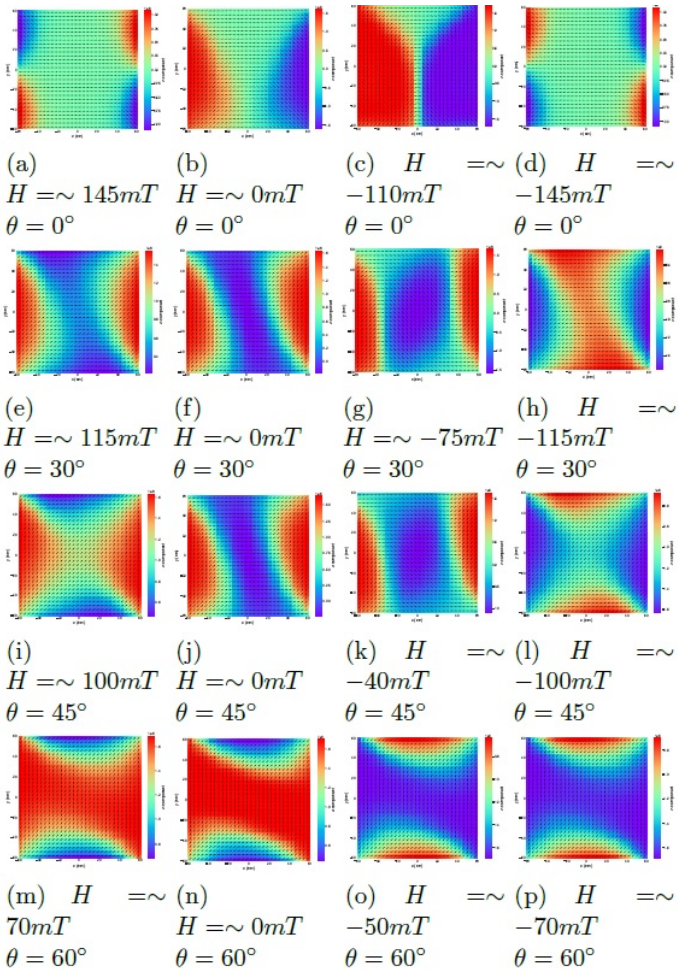

FIGURE 6. *Magnetization diagrams for $L = 120$ nm and $t = 9$ nm. 0°: a) $H \sim 145mT$, b) $H \sim 0mT$, c) $H \sim -110mT$ and d) $H \sim -145mT$. 30°: e) $H \sim 115mT$, f) $H \sim 0mT$, g) $H \sim -75mT$ and h) $H \sim -115mT$. 45°: i) $H \sim 100mT$, j) $H \sim 0mT$, k) $H \sim -40mT$ and d) l) $H \sim -100mT$. 60°: m) $H \sim 70mT$, n) $H \sim 0mT$; o) $H \sim -50mT$ and p) $H \sim -70mT$.*

pointing into the plane for H $\sim$ -110 mT. The magnetization reversal process has already started, resulting in most of the magnetic moments being mostly distributed in two large magnetic domains, with a Néel domain wall in between, one on the left side of the cuboid pointing vertically and upwards in a region where the magnetization has a component pointing out of the plane, and the

other one on the right side of the cuboid, pointing vertically and downwards.

As for the magnetic configurations for other angles and some selected field values, they are shown in Figures 6 (e) to (p). What is evident is that, as we move, the direction of the field away from the easy axes, the morphology of the magnetic domains changes and it is characterized in general by a reorientation of the magnetic moments as a result of the interplay and competition among the different energies. In particular, regions with a z-component of the magnetization are more marked, the surface associated to the domain walls increases and the walls are even wider.

Moreover, the number of Néel walls seems to be duplicated compared to the case with $\theta = 0°$, which is more evident at those field values close to coercivity.

Conclusions

In this work, we have addressed the effect of the spatial geometry of an applied uniform external magnetic field, upon the magnetic properties of Fe cuboids of submicron dimensions. Such geometrical feature was taken into account through the angle θ formed by the external field vector and one of the easy axes of the single crystal Fe sample. Results allow us to conclude that the coercive force is strongly influenced by geometry, which is an important factor to consider for technological applications. More concretely, coercive force exhibits a trend to decrease with the angle θ before the next easy axis is attained. During that process, a particular feature was observed at $\theta = 30°$ and $\theta = 60°$, where the anisotropy energy at the coercive field is smaller than that at the saturation field. This fact was attributed to the increase of accessible paths in phase space along which the system executes magnetization reversal and demonstrates the complexity of the energy landscape. Finally, a detailed balance of the various energies involved, their orders of magnitude and, therefore, their relative weights, as well as the snapshots of the magnetic moments or magnetic congurations, were also taken into account.

Acknowledgments

J.R. - M.G. acknowledges University of Antioquia for the exclusive dedication program. Financial support was provided by the CODI-UdeA 2017-16253 and 2020-34211 projects.

References

[1] U. Khan, A. Akbar, U. Ahmad, S. Riaz, and S. Naseem, Materialstoday: proceedings **2**, 5421 (2015).

[2] S. Mulenko, Y. N. Petrov, and N. Gorbachuk, Appl. Surf. Sci. **258**, 9186 (2012).

[3] S. Rani, S. C. Roy, N. Karar, and M. Bhatnagar, Solid State Commun. **141**, 214 (2007).

[4] C. Luna and R. Mendoza, Ingenierías **16**, 6 (2013).

[5] C. Blanco, *Magnetic interactions in rare earth-transition metal systems and their study by synchrotron radiation techniques.* (Tesis - Repositorio Institucional de la Universidad de Ovi, 2017) p. 212.

[6] K. Y. Guslienko, V. Novosad, Y. Otani, H. Shima, and K. Fukamichi, Appl. Phys. Lett. **78**, 3848 (2001).

[7] X.-T. Tang, G.-C. Wang, and M. Shima, IEEE T. Magn. **42**, 2975 (2006).

[8] M. B. Hahn, J. Phys. Commun. **3**, 075009 (2019).

[9] G. S. Abo, Y. Hong, J. Park, J. Lee, W. Lee, and B. Choi, IEEE T. Magn. **49**, 4937 (2013).

[10] M. J. Donahue and M. Donahue, *OOMMF user's guide, version 1.0* (NIST, 1999).

[11] L. Landau and E. Lifshits, Ukr. J. Phys. **56**, 51 (2008).

[12] M. Kirschner, T. Schrefl, F. Dorfbauer, G. Hrkac, D. Suess, and J. Fidler, J. Appl. Phys. **97**, 10E301 (2005).

[13] E. A. Jagla, Phys. Rev. B **72**, 094406 (2005).